SPECIAL ISSUE | RESEARCH PAPER
https://doi.org/10.1071/WF22109

International Journal of WILDLAND FIRE

International Association of Wildland Fire

KAPAS II: simulation of peatland wildfires with daily variations of peat moisture content

Dwi M. J. Purnomo[A], Sebastian Apers[B], Michel Bechtold[B], Parwati Sofan[C] and Guillermo Rein[A,*]

For full list of author affiliations and declarations see end of paper

*Correspondence to:
Guillermo Rein
Department of Mechanical Engineering, Leverhulme Centre for Wildfires, Environment and Society, Imperial College London, London, SW7 2AZ, UK
Email: g.rein@imperial.ac.uk

Received: 29 June 2022
Accepted: 10 March 2023
Published: 21 April 2023

Cite this:
Purnomo DMJ *et al.* (2023)
International Journal of Wildland Fire
32(6), 823–835. doi:10.1071/WF22109

ABSTRACT

Background. Peatland wildfires involve flaming vegetation and smouldering peat. The smouldering behaviour strongly depends on peat moisture, which can change significantly and quickly due to weather or human activities. **Aims.** We simulated wildfire in peatlands at the field scale and, for the first time, included daily variations of peat moisture. **Methods.** We developed KAPAS II, a cellular automaton that includes flaming and smouldering, and coupled it with PEATCLSM (Catchment Land Surface Model) for peatland hydrology. **Key results.** Compared with the satellite observations over 90 days of a 2018 wildfire in Borneo, KAPAS II predictions provide good agreement for burn scars (79% accuracy) and for the number of smouldering hotspots (85% accuracy). For the same burn scar, the model predicts that 54 ha of peat would smoulder when considering daily moisture variations, but only 12 ha if moisture was constant. Simulations at the same Borneo location, but in different years from 2000 to 2019, show the importance of seasons and climate events like El Niño. **Conclusion.** Temporal variations in peat moisture, which are strongly influenced by weather and climate, are important to predict the behaviour and severity of peatland wildfires. **Implications.** This model improves our understanding of wildfire behaviour in peatlands and can contribute to its mitigation.

Keywords: cellular automaton, fire, KAPAS, modelling, moisture, peat, smouldering, soil, wildfire.

Introduction

Peatland wildfires release carbon stored in peat, thus resulting in a positive feedback that contributes to climate change (Rein 2013). These wildfires involve both flaming and smouldering, with flames mainly burning surface vegetation (such as trees, shrubs, crops and grasses) and smouldering mainly burning peat, the organic soil underneath the vegetation. Smouldering wildfires can be sustained for weeks to months (Rein 2013; Turetsky *et al.* 2015; Lin *et al.* 2019; Rein and Huang 2021). Compared with flaming, smouldering spreads more slowly and at a lower temperature but releases a higher yield of pollutants, both gas and particulate matter (Rein 2013; Hu *et al.* 2018). An example where the importance of smouldering is clear is the 1997 peatland wildfires in southeast Asia. These wildfires emitted 0.8–2.56 Gt C (gigatonnes of Carbon) to the atmosphere, which is equivalent to 13–40% of global anthropogenic carbon emissions in that year, but only ~0.1 Gt C of these emissions resulted from flaming (Page *et al.* 2002).

The peat moisture content (MC), which in this paper is referred to as the gravimetric MC if not stated otherwise, plays a prominent role in the behaviour of smouldering wildfires (Rein 2013; Christensen *et al.* 2020; Lin *et al.* 2021). In natural peatlands, the peat MC changes temporally owing to weather and seasonal variations that can be increased by anthropogenic activities (Waddington *et al.* 2015; Bechtold *et al.* 2020; Goldstein *et al.* 2020). Because these temporal variations can be large within a short time span (daily, even hourly, Waddington *et al.* 2015; Bechtold *et al.* 2020; Goldstein *et al.* 2020) and because smouldering wildfires can sustain themselves for weeks to months (Rein 2013; Scholten *et al.* 2021), understanding the effects of temporal peat MC variations on smouldering behaviours is important.

Research on smouldering wildfires at the field scale is limited (Purnomo *et al.* 2021; Widyastuti *et al.* 2021; Yuan *et al.* 2021). The complexity and spatiotemporal extents of peatland wildfires prevent state-of-the-art wildfire models from properly simulating these phenomena. While physics-based computational models (e.g. computational fluid dynamics models) are too computationally expensive for field-scale scenarios (Purnomo *et al.* 2021), semiphysical and empirical models (e.g. the Fire Area Simulator model; Finney 1998) lack the ability to couple flaming and smouldering (Purnomo *et al.* 2021).

Here, we used cellular automata (CA), which use simple rules rather than complex physics-based equations (von Neumann 1967; Wolfram 1984), to simulate peatland wildfires that involve both flaming and smouldering. Despite being simpler than other models and thus requiring fewer equations and fewer resources, sufficiently accurate results can be achieved with CA (Alexandridis *et al.* 2008; Fernandez-Anez *et al.* 2019). CA consider a grid of cells that can be in different states (e.g. unburned, burning, or burned). The state of each grid cell is updated at discrete time steps by following a set of simple rules.

Purnomo *et al.* (2021) successfully simulated both flaming and smouldering in peatland wildfires at the field scale over a 3-month period; however, they did not consider temporal variations in peat MC. Owing to the long lifespan of smouldering wildfires and the significant changes in peat MC that can occur within a short time span, the model produced in Purnomo *et al.* (2021), KAPAS,[1] insufficiently captured realistic peatland conditions and thus led to inaccurate simulations. In addition, KAPAS can be used with only one set of spatial and temporal resolutions in the computational domain, which must be equal to the resolutions used in the model calibration. Each time the simulation requires a different spatial or temporal resolution, KAPAS must be recalibrated with this new resolution; otherwise, its predictions could become unrealistic (e.g. resulting in smouldering that spreads a few orders of magnitude faster than the expected spread rate). This problem occurs in most CA fire models (Purnomo 2022).

Here, we further developed KAPAS to simulate field-scale peatland wildfires by integrating temporally varying peat MC and allowing simulations at any spatiotemporal resolution. We used remote sensing data to derive the model input parameters (e.g. the vegetation type and density) and a peat-specific land surface model to estimate the temporal peat MC variations. We validated our CA model against satellite observations of burn scars, which in this paper are referred to as flaming burn scars if not stated otherwise, and smouldering hotspots. We then used our model to investigate the effects of daily and seasonal peat moisture variations on smouldering wildfires over contrasting climatic conditions.

Materials and methods

Cellular automata

CA are discrete computational models that use simple rules to simulate physical phenomena (von Neumann 1967; Wolfram 1984). In these models, the domain is a matrix of cells in which each grid cell can be in one of n discrete states that is updated at discrete time steps. The updating process of these states follows a set of rules (e.g. stochastic, empirical and physical rules) that affects both the cell and its nearby cells (called a *neighbourhood*). The set of rules and the neighbourhood are selected based on the phenomenon being simulated (Karafyllidis and Thanailakis 1997; Belcher *et al.* 2010; Collin *et al.* 2011; Fernandez-Anez *et al.* 2019).

In the initial work on modelling peatland wildfires with CA, the KAPAS model developed in Purnomo *et al.* (2021) employed stochastic rules called *bond percolation*. In the bond percolation concept, the flow of information from one entity to adjacent entities occurs with a certain probability (Favier 2004; Purnomo 2022). In the context of wildfire modelling, the bond percolation concept allows a fire to spread from one cell to adjacent cells with a certain probability representing the flammability of the fuel, where higher probabilities correspond to higher fuel flammability levels, thus facilitating a faster spread rate (Purnomo 2022). Owing to the probabilistic rules in the bond percolation CA model, when this model is run repeatedly with identical input parameters, the simulation results reflect stochastic uncertainty, and the results obtained from multiple repetitions (of simulations with identical input parameters) differ. This trait can mimic the uncertainty observed in nature, for example the uncertainty caused by landscape heterogeneity.

In this work, we used the bond percolation rules with a Moore neighbourhood (in which the eight cells directly surrounding a considered cell are included in the neighbourhood, forming a 3×3 square grid), similar to that used in KAPAS (Purnomo *et al.* 2021). However, we implemented significant modifications to these rules to improve the accuracy and applicability of KAPAS. We refer to the updated model as KAPAS II, as this new model has a similar approach and is used for the same purpose as the initial KAPAS model (to model flaming and smouldering wildfires) developed in Purnomo *et al.* (2021).

States and rules of the KAPAS II model

KAPAS II considers the same five possible states as the model developed in Purnomo *et al.* (2021) for each cell: *surface vegetation* (*SV*), *flaming vegetation* (*FV*), *exposed peat* (*EP*), *smouldering peat* (*SP*) and *burned peat* (*BP*) (Fig. 1). *EP* represents a state in which the cell has lost its surface

[1]Modified abbreviation of **CA** for **F**laming **A**nd **S**mouldering that also means 'cotton' in the Indonesian language, as cotton is a material that can facilitate both flaming and smouldering.

vegetation owing to flaming but has intact peat soil because smouldering peat fails to ignite.

At the initial time step ($t = 0$), the fire is ignited at a specific location to initiate the *FV* state. The *FV* cells then ignite the neighbouring vegetation with a probability of P_f and may ignite the underlying peat (*SP*) with a probability of P_t (see Fig. 1). A higher P_f value corresponds to a faster flaming spread rate, whereas a higher P_t value corresponds to nucleation (i.e. multiple ignitions of hotspots that arise at randomly distributed locations) of more smouldering hotspots. If the *FV* fails to ignite the peat, the cell adopts the EP state. An SP cell spreads at a rate dependent on the P_s value (smouldering spread probability) and eventually extinguishes with a probability of P_e, thus becoming *BP*.

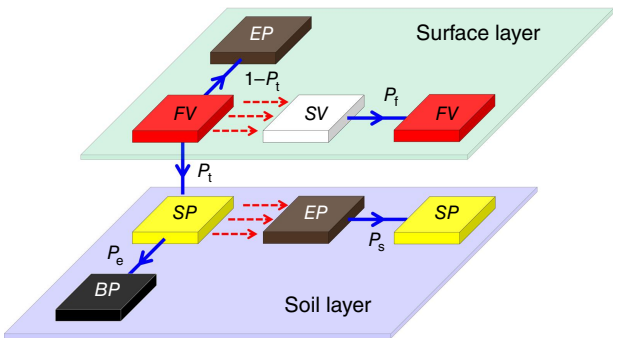

Fig. 1. The states and rules of KAPAS II. *FV* is flaming vegetation, *SV* is surface vegetation, *SP* is smouldering peat, *EP* is exposed peat, *BP* is burned peat, P_f is the probability of the flames spreading, P_t is the probability of the transition from flaming to smouldering occurring, P_s is the probability of smouldering spreading, and P_e is the probability of smouldering extinguishing. The solid arrows represent possible state changes, whereas the dotted arrows represent potential influences from neighbouring cells. This figure was adapted from KAPAS in Purnomo *et al.* (2021).

Following Fernandez-Anez *et al.* (2019) and Purnomo *et al.* (2021), in the KAPAS II model, we use separate surface and soil layers in the cells (see Fig. 1) to enable the simulation of smouldering spread underneath unburned vegetation or firebreaks (if a flammable peat layer is present between a firebreak and the water table or mineral soil). By applying two separate layers, the cells in the soil layer can become smouldering peat, although in the surface layer, neither unburned vegetation nor firebreaks change state. The transition of flaming vegetation on the surface resulting from underlying smouldering is not considered in KAPAS II, as this would require the inclusion of additional rules involving the transition from smouldering to flaming, which misses the objective of KAPAS II. The flaming of peat is unlikely (Huang and Rein 2015; Lin *et al.* 2019); thus, it is not considered in KAPAS II.

Input parameters and validation datasets

We simulated a peatland wildfire in Borneo (located at 3.087°S, 113.991°E) that started on 21 September 2018 and was fully extinguished on 10 October 2018, which was selected owing to the availability of the data. Fig. 2 shows the progression of the flaming wildfire captured by the Sentinel-2 satellite (Copernicus 2022). These satellite images were obtained by using false-colour urban composites that clearly distinguish among surface vegetation, burn scars and flames (Stavrakoudis *et al.* 2020). The black colour in Fig. 2 represents the burn scar, whereas the red areas represent regions of flames. The light green colour represents a non-combustible region such as a firebreak or burned area that resulted from previous wildfires that were not considered in this research.

The data obtained from Sentinel-2 were used to estimate the burn scar in the validation process. In the model, the shape formed by *EP* cells corresponded to the burn scar. We

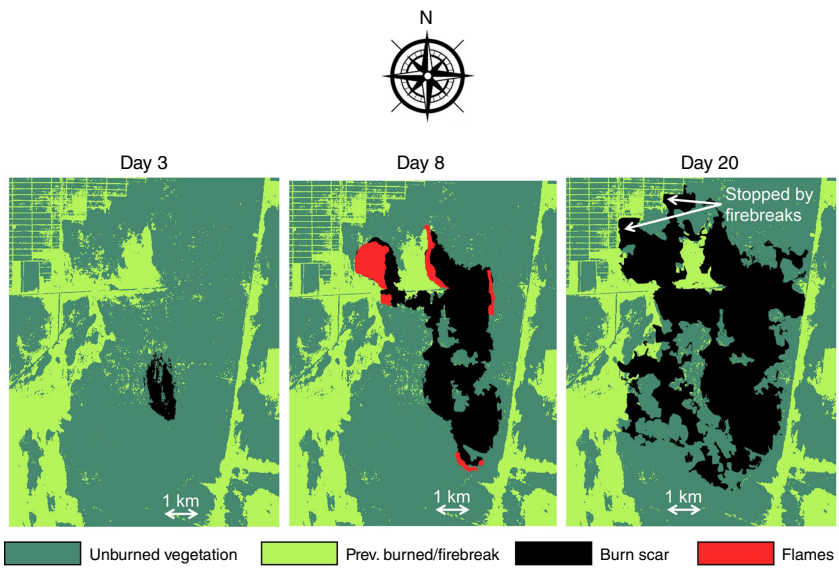

Fig. 2. Satellite image of a landscape in Borneo (3.087°S, 113.991°E) in September 2018, obtained from Sentinel-2 (Copernicus 2022), which shows the progression of flames and the burn scar.

used the seed-fill algorithm (Khayal *et al.* 2011) to detect burn scar pixels (black colour) from the satellite images shown in Fig. 2. The burn scar also shows the locations of firebreaks, which serve to stop flames from spreading. Firebreaks are indicated by the abrupt stop of a flaming wildfire, thus causing the burn scar to exhibit smooth edges (see Day 20 in Fig. 2). Fig. 3*a* shows the landscape distribution, including the estimated locations of firebreaks before the flames began (on 8 September 2018).

KAPAS II considers three different surface vegetation types: dry shrubs, wet shrubs and trees (shown in Fig. 3*b*), following Ferraz *et al.* (2019), who used field sampling and satellite observations to estimate vegetation types. KAPAS II also considers the rain and wind conditions to simulate flaming wildfires. We used meteorological data from a local weather station to obtain daily precipitation, wind speed and wind direction data (measured 6 m above the surface). This weather station is located at 2.220°S, 113.951°E, ~93 km north of the landscape under study (BMKG 2018). For the wind direction, we used the convention of direction of origin; thus, for instance, a south-eastern wind describes wind coming from the southeast and moving northwest. These meteorological phenomena significantly change over short time spans (hourly or even shorter); however, these daily data are the only locally available data. KAPAS II can be run with higher temporal resolution of meteorological data (e.g. hourly) if available.

We considered the vegetation density in KAPAS II (see Fig. 4). We classified the vegetation density based on Normalized Difference Vegetation Index data (NDVI, a surface vegetation greenness index) as shown in Fig. 4*a*, which are commonly used to estimate vegetation density (Camps-Valls *et al.* 2021), obtained from Sentinel-2 (Copernicus 2022). However, we considered only three classes of vegetation density, recently burned, regrown or intact vegetation, corresponding to the methods of Alexandridis *et al.* (2008). Therefore, the values shown in Fig. 4*a* were reclassified into three classes: values ranging from 0 to 0.2 corresponded to recently burned vegetation, 0.2–0.4 indicated regrown vegetation, and 0.4–0.65 indicated intact vegetation (as shown in Fig. 4*b*). Recently burned vegetation corresponds to vegetation that was burned in recent previous wildfires; regrown vegetation corresponds to previously burned vegetation that has started to regrow; and intact vegetation refers to fuel that has not been affected by recent wildfires (see Fig. 3*a*, in which the green colour in the landscape consists of dark and light greens). Fig. 4*c* shows the vegetation density classification used in the model. Although the entire region in the landscape under study consists of peatlands, the black region in Fig. 4*c* was not considered in the model because it is completely separated by firebreaks (see Fig. 3*a*), inhibiting flame spread into the black region. We selected NDVI data collected at the start of the wildfire (on 21 September 2018), and therefore, the data represented the actual ground conditions.

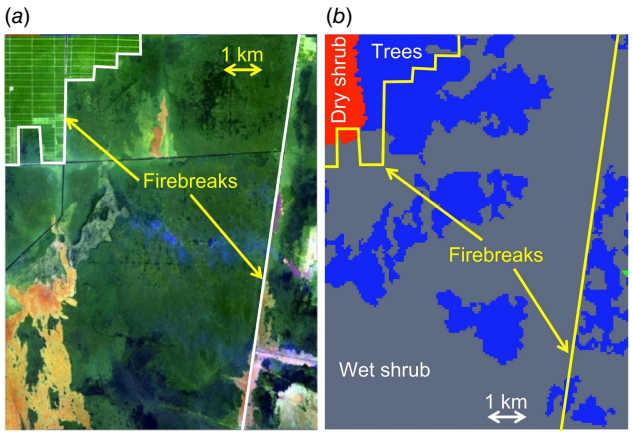

Fig. 3. (*a*) Satellite image of a landscape in Borneo (3.087°S, 113.991°E) in September 2018 before the flames began; this image was obtained from Sentinel-2 (Copernicus 2022). The white lines highlight firebreaks. (*b*) Remote sensing-based vegetation types identified in the peatlands in the Borneo landscape (3.087°S, 113.991°E), as obtained from Ferraz *et al.* (2019). We considered three vegetation types: dry shrubs (red), wet shrubs (grey) and trees (blue). The yellow lines show firebreaks, corresponding to the white lines in panel (*a*).

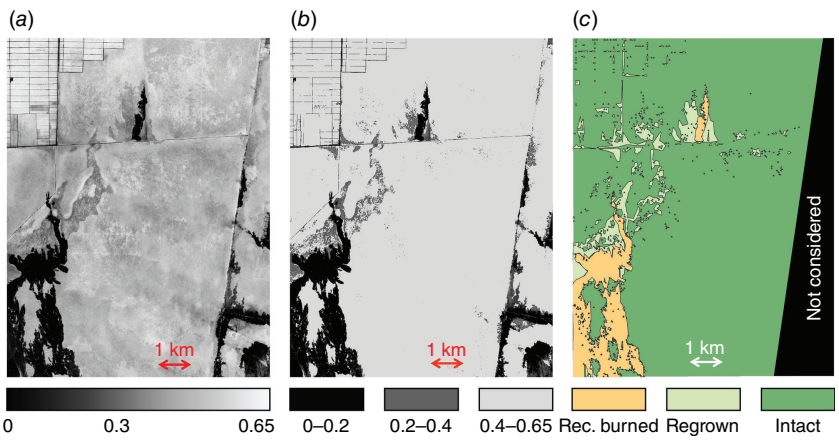

Fig. 4. (*a*) The NDVI data of a landscape in Borneo (3.087°S, 113.991°E) on 21 September 2018; these data were used to estimate the vegetation density, and were obtained from Sentinel-2 (Copernicus 2022). (*b*) Reclassified NDVI data in the same landscape at the same date; these data were used to simplify the vegetation density classification scheme and were adapted from Alexandridis *et al.* (2008). (*c*) The vegetation density data characterising the same landscape at the same date, which were used in the model; these data were based on the NDVI data and classified as recently burned (rec. burned), regrown, or intact. The black region was not considered because it was separated by a firebreak.

The peat MC data were obtained from simulations conducted with the peat-specific land surface model in Apers *et al.* (2022), using the tropical version of the peat-specific land surface model developed by Bechtold *et al.* (2019). The model in Apers *et al.* (2022) was specifically developed and extensively evaluated for tropical peatland conditions and was shown to perform best over southeast Asian peatlands. This model was based on the Catchment Land Surface Model (CLSM) of the NASA GEOS (Goddard Earth Observing System) Earth System Modelling framework and has two modules, one for drained tropical peatlands (PEATCLSM$_{Trop,Drain}$) and one for natural tropical peatlands (PEATCLSM$_{Trop,Nat}$); these different peatland types have distinct hydrological conditions and thus have different peat MC characteristics (Apers *et al.* 2022). Canal construction had been under way in central Kalimantan since the 1990s (Ritzema *et al.* 2014), and we found a number of canals inside our study area based on the canal map produced by Dadap (2020); therefore, we assumed that the peatland under the study area was drained. From this assumption, the PEATCLSM$_{Trop,Drain}$ model in Apers *et al.* (2022) was used to obtain the peat MC data for KAPAS II. We used the soil surface MC (0–5 cm depth) instead of a deeper MC, because the ignition of smouldering wildfires most of the time occurs at the surface.

The MC information obtained from the model in Apers *et al.* (2022) was volumetric (volume-based), whereas that used in KAPAS II is gravimetric (mass-based). Thus, to obtain gravimetric MC data, we divided the volumetric MC by the peat bulk density (in g/cm^3). The peat bulk density is a function of the peat solid density and porosity. We assumed the peat solid density to be 1.5 g/cm^3, adopting the value reported by Huang and Rein (2017). The porosity of peat in natural peatlands varies significantly with depth; at the surface, porosity can exceed 0.8, whereas at deeper points (~50 cm), it can be less than 0.5 (Rezanezhad *et al.* 2016). Although the peat porosity described in Rezanezhad *et al.* (2016) corresponds to non-tropical peat, a study in Indonesian tropical peatlands revealed that the peat porosity at a 50 cm depth was approximately 0.41 (Islami *et al.* 2018). In KAPAS II, we selected the average of surface (0.8) and deep (0.41) peat porosity values; thus, a porosity of 0.61. This value is lower than 0.9 (Huang and Rein 2015), the commonly used value in smouldering models that focus on the porosity of surface peat. However, the peat porosity used in KAPAS II is similar to that used in Apers *et al.* (2022) (0.68). From these selected values, the peat bulk density in KAPAS II is 0.585 g/cm^3; thus, the obtained volumetric MC was divided by 0.585 to convert to gravimetric MC.

Whereas we used satellite burn scar data to validate the flaming component in the KAPAS II model, we used a remote sensing algorithm developed by Sofan *et al.* (2020), called Tropical Peatland Combustion ALgorithm (ToPeCAL), to detect smouldering hotspots to validate the smouldering model component. ToPeCAL performs arithmetic and logic operations on short-wave infrared (SWIR) data from Sentinel-2 to detect smouldering wildfires that are separated from flaming wildfires. Fig. 5 shows the smouldering hotspots that were detected using ToPeCAL and used to validate the smouldering component of the KAPAS II model. However, we consider only the number of smouldering hotspots, rather than the shape of the smouldering burn scar (which is the output of ToPeCAL) when validating our model. This indicates that we validated the model based only on the ignition of smouldering without considering smouldering spread. We did not validate the spread because it can occur undetected and even in the subsurface, thus invalidating detection results obtained via satellite remote sensing.

Model calibration

KAPAS II predictions are dependent on the values of the main probabilities (P_f, P_t, P_s and P_e). P_f (Eqn 1) is a function of the flaming spread rate (R), spatiotemporal resolution (λ), vegetation density factor (α_d) and wind factor (α_w). The λ term contains the information of the cell size (Δx) and time step (Δt) and is formulated in Eqn 2. R is formulated based on the Rothermel model for flame spread (Rothermel 1972) under no-wind conditions. Table A1 in the appendix lists the values of input parameters used to calculate R. R is translated into a probability value depending on λ, which then becomes the base value of P_f (i.e. if α_d

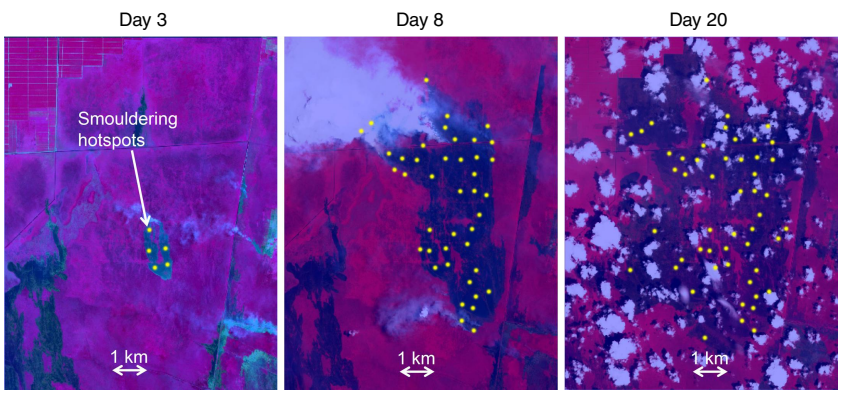

Fig. 5. The smouldering hotspots (yellow circles) in a landscape (in Fig. 3) in Borneo (3.087°S, 113.991°E) in 2018 detected by the algorithm developed by Sofan *et al.* (2020) and applied on Sentinel-2 data (Copernicus 2022). The increase in the number of hotspots corresponds to the progression of the flaming wildfire (see Fig. 2).

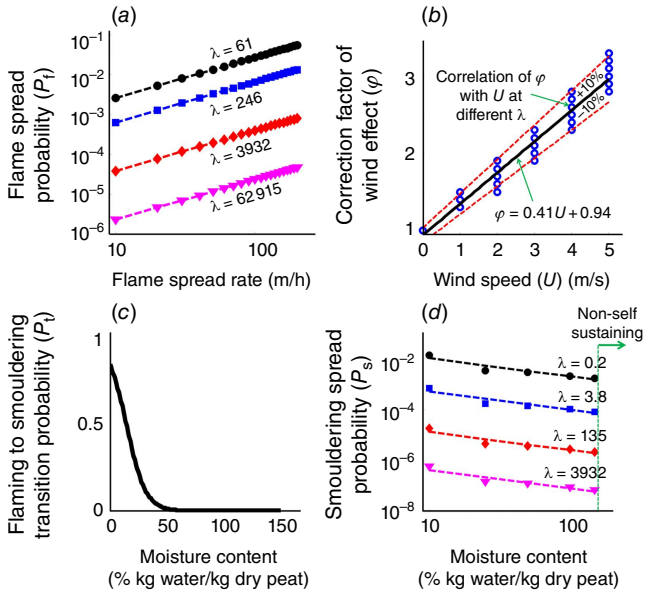

Fig. 6. The calibration of variables in KAPAS II at different spatiotemporal resolutions (cell size per time step) of the computational domain (λ). (*a*) The translation of the flame spread rate, based on the Rothermel model calculation, into a probability value, P_f, at different λ values. (*b*) The correlation between the wind speed (U) and the correction factor of the wind effect (ϕ) at different λ values. (*c*) The correlation between the probability of a transition from flaming to smouldering occurring and the MC, adapted from Frandsen (1997). (*d*) The relationship between smouldering spread probability and the MC at different λ values, calibrated against experimental data (Huang *et al.* 2016; Prat-Guitart *et al.* 2016).

and α_w are equal to 1). This translation was performed by optimising the probability value to have KAPAS II predict flaming spread rate of R given the cell size and time step. Fig. 6*a* clearly shows that R and the base P_f value reflect a log–log relationship with slopes independent of λ. With this method, any cell size and time step can be used in the model with a less than 15% relative absolute error, thus significantly improving the previous model (KAPAS) developed in Purnomo *et al.* (2021).

$$P_f = \alpha_w \alpha_d e^{-4.12}\left(\frac{R}{\lambda}\right)^{1.02} \quad (1)$$

$$\lambda = \frac{\Delta x}{\Delta t} \quad (2)$$

KAPAS II considers the effect of wind (α_w) as formulated in Eqn 3. α_w is based on the wind factor formulation by Rothermel for the maximum downwind spread rate and on the 2D propagation behaviour (Rothermel 1972; Alexander 1985; Finney 1998). α_w is a function of the wind coefficient (Φ_w), the direction of flame spread relative to the wind direction (θ), the ellipse parameters: semiminor axis (a), semimajor axis (b), and linear eccentricity (c), and the correction factor (φ). Φ_w is determined based on the Rothermel model, whereas the ellipse parameters are formulated using Eqns A1–A3 in the appendix and depend on the wind speed (U) following Finney (1998). These formulation represent an improved version of the wind effect in KAPAS (Purnomo *et al.* 2021), because KAPAS did not maintain an elliptical shape under high wind speeds.

$$\alpha_w = \varphi\left(\frac{a^2}{b - c\cos\theta}\right)\Phi_w \quad (3)$$

The correction factor of the wind effect (φ) is required to maintain agreement in the downwind spread rate with Rothermel. Without this correction factor, the spread rate differs significantly, up to 90%. From the calibration, we found that φ is linearly correlated with U, as shown in Eqn 4, and the variations that arise owing to different λ values remain within 10% (see Fig. 6*b*).

$$\varphi = 0.41U + 0.94 \quad (4)$$

The effect of the vegetation density (α_d), which was not considered in KAPAS, is determined by calibrating the model against satellite-derived burn scar data. KAPAS II considers three different vegetation density classes (intact, regrown and recently burned), and the α_d value for regrown vegetation was calibrated. The α_d value for intact vegetation was set to 1, and that for recently burned vegetation was set to 0 for the sake of simplicity. From the calibration process, we found that for $\alpha_d = 0.01$ for the regrown vegetation, flame spread predictions provide good agreement with the satellite-derived burn scar data (<25% relative absolute error).

The flaming to smouldering transition probability (P_t) and smouldering extinction probability (P_e) values in KAPAS II were set following KAPAS. P_t is a function of peat MC, as in Eqn 5, using the ignition probability formulated in Frandsen (1997) (see Fig. 6*c*), and P_e is selected to be 5×10^{-10}, sustaining a smouldering fire for approximately 3 months (the typical duration of the wildfire season in Indonesia; Huijnen *et al.* 2016). The formulation of smouldering spread probability (P_s) in KAPAS II was also adapted from KAPAS and the values fit the experiments of Huang *et al.* (2016) and Prat-Guitart *et al.* (2016); however, different spatiotemporal resolution values (λ) were input into KAPA1S II to enable modelling at any spatial or temporal resolution of the computational domain (thus improving the KAPAS model). We found that P_s is linearly correlated in log–log axis with MC ($R^2 = 0.89$) and has a slope independent of λ (see Fig. 6*d*); P_s is formulated in Eqn 6. The MC values used in Eqns 5, 6 change daily based on the model in Apers *et al.* (2022); thus, P_t and P_s also change daily. KAPAS II considers temporal variations in peat MC but assumes it is spatially uniform across the entire landscape. Peat MC also varies spatially (Prat-Guitart *et al.* 2017); however, whereas the spatial peat MC variations can be considered in KAPAS II, there are currently no reliable peat moisture data at fine

spatial resolution and the resolution of the model in Apers *et al.* (2022) was too coarse for the landscape under study (5-km resolution).

$$P_t = (1 + 0.17e^{0.12MC})^{-1} \quad (5)$$

$$P_s = 0.01MC^{-0.71}\lambda^{-1.02} \quad (6)$$

In this work, we used a domain with a 45-m cell size and a 1200-s time step ($\lambda = 135$ m/h). To limit computational costs, we selected the coarsest cell size that still gave a higher than 80% accuracy on flaming and smouldering spread rate predictions, resulting in the domain having ~200 000 cells. The time step was determined based on the stability criteria of Courant–Friedrichs–Lewy to avoid the diffusion of any entity exceeding one cell at one time step (Lautenberger 2013).

We verified the KAPAS II predictions in a simpler domain of uniform fuel with constant wind. We compared KAPAS II spread rate predictions of the flames for different wind speed with the Rothermel model (Fig. A1*a*) and of the smouldering at different moisture content with the experiments of Huang *et al.* (2016) and Prat-Guitart *et al.* (2016) (Fig. A1*b*). We found that for both flaming and smouldering spread, KAPAS II predictions are within 20% relative absolute error of the benchmarks.

Results and discussions

Fig. 7 shows snapshots of KAPAS II predictions at four different times from Day 3 to Day 90. Fig. 7*a–c* corresponds to the spread of flames, whereas Fig. 7*d* corresponds to the spread of smouldering. On Day 3 after the start of the wildfire (Fig. 7*a*), flames had burned a relatively small area of surface vegetation, and the shape of the burn scar was quite circular, with non-smoothness at the perimeter caused by the stochastic approach of KAPAS II. The south-eastern wind of 7 km/h had only a slight effect on the burn scar. On Day 8 (Fig. 7*b*), the western wind (see Fig. 4) caused eastward spread of the flames. The low vegetation density caused the formation of an unburned patch in the north of the burn scar. Smouldering hotspots began to form at this stage. We refer to the smouldering hotspots formation by flames as nucleation, and smouldering spread grows these hotspots. On Day 20 (Fig. 7*c*), all flames had become extinguished, and the nucleation of smouldering hotspots stopped. KAPAS II predicted that the flames were extinguished on Day 15. For comparison purposes, Fig. 7*c* shows a snapshot of Day 20, a day for which a clear satellite image was available (on the other days, satellite images were either unavailable or significantly cloud-covered). The extinction of the flames corresponded with 14.7 mm of precipitation on Day 15. This precipitation continued for 3 days. Therefore, we argue that the flames and hotspot nucleation lasted for 16 days (Day 0–15). From Day 16, hotspots started to spread and grew larger, and at the end of the simulation on Day 90, the hotspots had significantly enlarged, and some had merged (Fig. 7*d*).

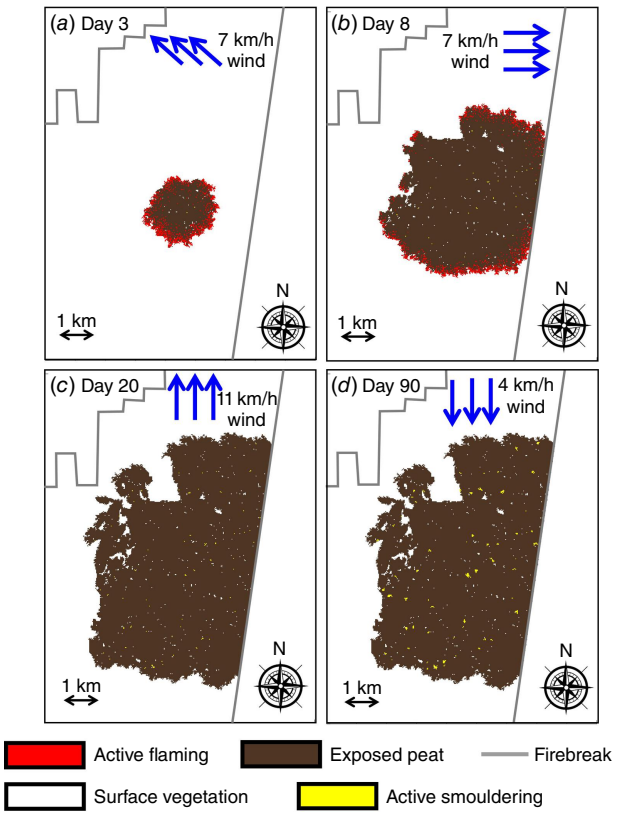

Fig. 7. Snapshots of the peatland wildfire simulation in the Borneo landscape (in Fig. 3, 3.087°S, 113.991°E) in 2018 at different stages: (*a*) early stage of surface flames on Day 3; (*b*) spread of surface flames and the nucleation of smouldering hotspots on Day 8; (*c*) extinction of surface flames and cessation of smouldering hotspot nucleation on Day 20; and (*d*) end of the simulation on Day 90, at which time the smouldering hotspots had enlarged and some merged. The surface vegetation (white) includes all three different vegetation types shown in Fig. 3*b*. The blue arrows show the wind speed and direction. Firebreaks (shown in grey) stopped the spread of flames but could not stop the spread of smouldering.

Fig. 8*a–c* shows a comparison between the satellite-based burn scars in Fig. 2 and those predicted by KAPAS II (Fig. 7*a–c*) at three different times (Days 3, 8 and 20). In the figure, the red lines represent the perimeter of the actual burn scar observed by the satellite. The true positive and true negative terms represent accurate predictions in which the burn scars observed by the satellite and predictions both indicated burned or unburned conditions, respectively. False positives correspond to an area that was predicted to be burned but was not burned in the satellite observation, and false negatives indicate regions that were not predicted to be burned but were observed to be burned by the satellite; both of these were considered inaccurate predictions. The flames burned approximately 8734 ha of vegetation in the 25 700-

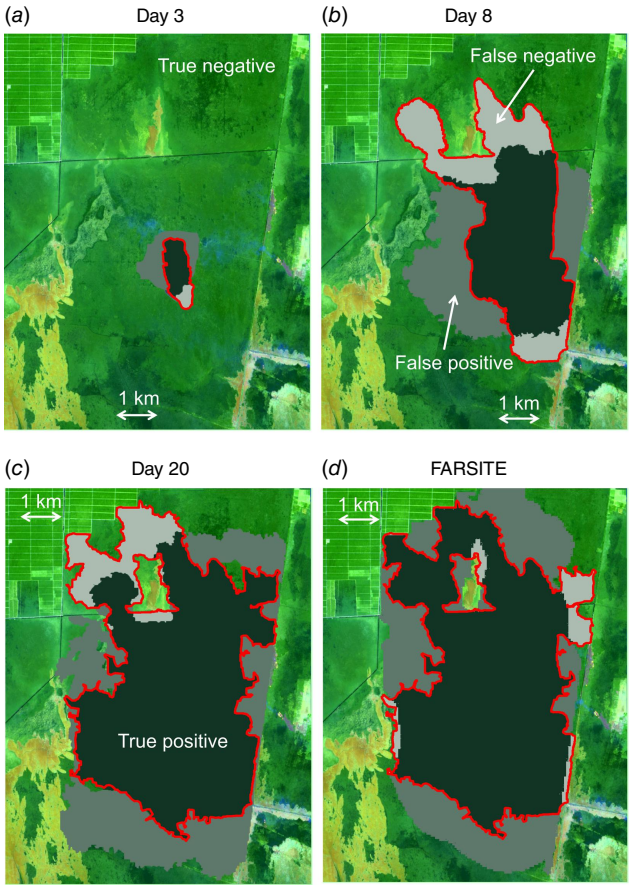

Fig. 8. Comparisons between the burn scars (exposed peat) derived from satellite detection (Fig. 2) and from the predictions of KAPAS II at three different times (*a*–*c*) and FARSITE on day 20 (*d*) in the Borneo landscape (in Fig. 3, 3.087°S, 113.991°E) in 2018. The red lines represent the perimeter of the actual satellite-detected burn scar. True negatives and true positives denote accurate predictions, indicating that the predicted and satellite-detected results both suggested not burned or burned regions, respectively. A false positive corresponds to a predicted burn region that was not burned in the satellite detection results, whereas a false negative indicates that an area was predicted to be a non-burned region but was found to be burned in the satellite detection results.

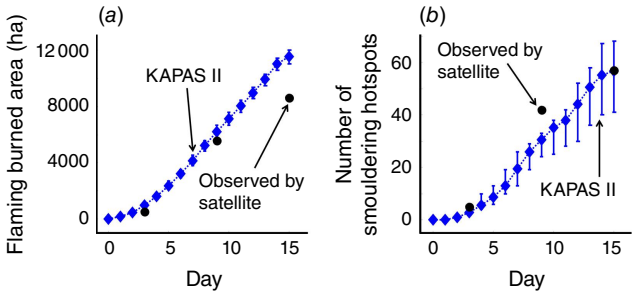

Fig. 9. (*a*) Comparisons between the flaming burned areas (areas of the exposed peat) derived from the satellite observations (based on Sentinel-2; Copernicus 2022) and from the KAPAS II predictions at different times. (*b*) Comparisons between the of numbers of smouldering hotspots derived from the satellite observations (based on Sentinel-2; Copernicus 2022) and the KAPAS II predictions at different times. The error bars represent the uncertainty of KAPAS II results after 10 repetitions.

ha study area. KAPAS II simulated the flame spread that resulted in burn scars with a 29.8% share of true positives, 49.2% true negatives, 16.9% false positives and 4.1% false negatives compared with the burn scar observed by the satellite at the end of the wildfire (Fig. 8*c*). Therefore, a Cohen's kappa value (a shape similarity indicator) of 0.57 was achieved, corresponding to reasonable agreement between KAPAS II predictions and observations (Sun *et al.* 2021). The main reason for the errors is the effect of wind. This can clearly be seen in Fig. 8*a*, *b*, where the burn scars observed by the satellite were elongated, whereas the simulated burn scars were significantly less elongated. We argue that this discrepancy resulted from KAPAS II considering the daily average wind speed and direction, whereas in reality, both the wind speed and direction vary significantly over the course of a day, especially when gusty winds occur. The flame spread predictions from KAPAS II were of similarly accuracy to the predictions from FARSITE (see Fig. 8*d*); FARSITE achieved a 32.9% share of true positives, 47.5% true negatives, 17.3% false positives and 2.3% false negatives, thus a Cohen's kappa value of 0.61.

We found that KAPAS II overestimated the burn scars by 30%, as KAPAS II predicted that flames burned 11 143 ha of vegetation (see Fig. 9*a*). After 16 days, the area burned by flames did not change; thus, it is not presented in Fig. 9*a*. We considered that the flames only lasted for 16 days (owing to precipitation); thus, both predictions and observations were compared based on Day 16 of flaming instead of Day 20 (Day 20 corresponds to the day clear satellite images were available). While flames spread, smouldering hotspots were nucleated, as shown in Fig. 9*b*. We validated the smouldering component of KAPAS II by comparing the number of smouldering hotspots at different times against satellite observations (see Fig. 5). The 61 predicted hotspots agreed well with the observed 53 hotspots, which means a relative error of 15%. KAPAS II is the only model that can predict nucleation accurately against satellite observations.

The discrepancies in the locations of hotspots between the predictions and observations may have stemmed from the actual spatial non-uniformity of peat MC, which is not considered in KAPAS II. This is supported by the number of new smouldering hotspots observed on Day 8 (42 new hotspots), which decreased over 75% on Day 16 (11 new hotspots), as shown in Fig. 5, although the burn scar from flames was similar, indicating that the region where flames spread during Day 8 had drier peat compared with the region within the burn scar on Day 16. Day 20 in Fig. 5 corresponds to Day 16 in this comparison because we argue that the flames stopped on Day 16. Meanwhile, KAPAS II predicted that the numbers of hotspots nucleated on Day 8

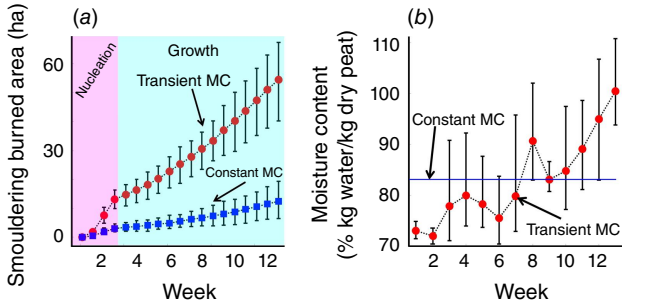

Fig. 10. (*a*) The predicted evolution of the smouldering burned area in the Borneo landscape (3.087°S, 113.991°E) over 90 days, under the assumptions of a constant peat MC (constant MC scenario, blue squares) or temporally varying peat MC (transient MC scenario, red circles). Under the nucleation regime (magenta), smouldering hotspot nucleation was found to be dominant over growth, whereas in the growth regime (cyan), smouldering spread (growth) was dominant. The error bars represent the uncertainty of the model results after 10 repetitions. (*b*) MC under the transient MC scenario averaged over 1 week and its range (error bars). The blue line denotes the MC averaged over 90 days, as used in the constant MC scenario.

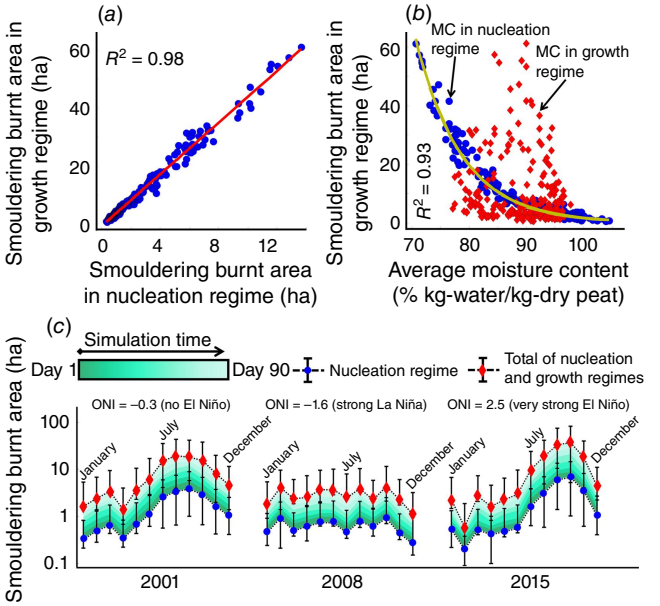

Fig. 11. Predicted smouldering burned area in the Borneo landscape (3.087°S, 113.991°E) when the flames began in different months and years between 2000 and 2019, under continuous simulation runs (even after flames were extinguished) lasting 90 days (time in the simulation). (*a*) Correlation between the smouldering burned areas identified under the nucleation and growth regimes. (*b*) Correlation of the smouldering burned area in the growth regime with the monthly average MC under the nucleation (blue circles) and growth (red diamonds) regimes. (*c*) Evolution patterns of the smouldering burned areas in different months and years. The total smouldering burned area (red diamonds) represent the sums of the smouldering burned area under the nucleation (blue circles) and growth (green gradient) regimes. The Oceanic Niño Index (ONI) determines the occurrence of El Niño and its counterpart, La Niña (Null 2021).

(27 hotspots) and Day 16 (34 hotspots) only differed by 25%.

Fig. 10*a* shows the evolution of the smouldering burned area. The magenta shade indicates the area under the smouldering nucleation regime (during flame spread), whereas the cyan shade indicates the area under the smouldering growth regime (after the flames were extinguished). Because of both nucleation and growth, the smouldering burned area increased exponentially with time, but this increase was slower during the growth regime than the nucleation regime. Overall, KAPAS II predicted that smouldering had burned a total of 54 ha of peat 90 days after the start of the wildfire.

Peat MC could significantly change over short time; for instance, as shown in the error bars in Fig. 10*b*, which represent the range of daily peat MC variations within 1 week. We analysed the importance of temporal peat MC variations by comparing the KAPAS II predictions with daily peat MC variations, a transient MC scenario, and the predictions with constant peat MC, a constant MC scenario. In the constant MC scenario, the peat MC was assumed to be constant at 83% kg water/kg dry peat (the average peat MC calculated over 90 days; see Fig. 10*b*). We found that the exponential increase of smouldering burned area in nucleation and growth regimes prevailed in both transient MC and constant MC scenarios. However, the smouldering area was significantly smaller in the constant MC scenario (12 ha) than in the transient MC scenario (54 ha). This finding emphasises the importance of implementing temporal peat MC variations.

We further used KAPAS II with transient MC to predict the smouldering burned area, nucleated over the same burn scar, if it happened in different months in the years 2000–2019. Each individual case runs for 90 days. A total of 240 cases were considered; the first case goes from January 2000 to March 2000, whereas the last case is from December 2019 to February 2020. Each of the cases had different temporal peat MC variations that were estimated with the drained version of the model in Apers *et al.* (2022) (see Fig. A2 for examples).

Fig. 11*a* shows that the smouldering burned area by growth regime is linearly proportional to the burned area by nucleation regime ($R^2 = 0.98$). However, Fig. 11*b* shows that the burned area by growth regime decreases exponentially with the monthly averaged peat MC during the nucleation period ($R^2 = 0.93$), but independent of the monthly averaged peat MC during the growth period ($R^2 = 0.05$). Therefore, the peat MC during the nucleation period is the crucial factor determining the total smouldering area. This inverse exponential correlation between peat MC during the nucleation period and smouldering burned area, which is highly dependent on the number of hotspots, agrees with the experiments of Frandsen (1997) in which the probability of a smouldering nucleation exponentially decreases with

MC. The maximum difference of peat MC identified between the nucleation and growth periods shown in Fig. 11*a*, *b* is less than 20%. Thus, this finding might not apply when a very large difference of peat MC occurs.

Fig. 11*c* shows the temporal evolution patterns of the smouldering areas predicted for different months and years. The smouldering area varied significantly and ranged from 0 to 93 ha. The smouldering area is minimal if the flames spread in the wet season, between November and May, and it significantly increases in the dry season. In the wet season, owing to the relatively high peat MC, smouldering hotspots were less likely to be nucleated; thus, some cases exhibited a smouldering area of 0 ha, whereas in the dry season, the peat became drier and more vulnerable to nucleation. This temporal pattern is mainly controlled by peat MC, thus strongly indicating the importance of temporal MC variations.

When a strong La Niña event occurred, the smouldering area was smaller than 10 ha throughout the year (see 2008 in Fig. 11*c*). During an El Niño event, the smouldering area significantly increased (see 2015 in Fig. 11*c*). The maximum smouldering area predicted for the dry season of a strong El Niño year (2015) was 93 ha, whereas in a year without El Niño (e.g. 2001), it was 48 ha (see Fig. 11*c*). The unique findings on the effect of different seasons on smouldering area indicate that seasonal peat MC variations, which are influenced by climate, determine the severity of smouldering wildfires.

Conclusions

We integrated CA and field data to simulate flaming and smouldering wildfires in peatland at the field scale in KAPAS II, and for the first time, we considered temporal peat MC variations. We simulated a peatland wildfire that occurred in Borneo in September 2018 and found that within 90 days, 54 ha of peat was affected by smouldering. When considering a constant peat MC, the smouldering burned area was significantly underestimated (12 ha), emphasising the importance of temporal peat MC variations.

We used KAPAS II to predict smouldering burned areas for fires that began in different months and years between 2000 and 2019 (240 cases); each case simulates 90 days. The smouldering burned area varied significantly and ranged from 0 to 93.4 ha; the area was below 10 ha if the flames began during the wet season and above 40 ha if the flames began during the dry season. We found that the nucleation of smouldering hotspot by flames is crucial for determining overall damage to peatlands. Wet peat during the nucleation period prevents the formation of smouldering hotspots and greatly minimises the overall damage.

In La Niña years, the smouldering burned areas are less than 10 ha throughout the year. In strong El Niño events, the smouldering burned area during the dry season would double compared with years without El Niño. For instance, in 2015 (a strong El Niño year), the smouldering burned area was 93 ha, whereas in 2001 (a year without El Niño), it was only 48 ha. These findings show that the significant seasonal peat MC variations, which are affected by climate, greatly determine the extent of smouldering wildfires. The modelling methods presented in this study provide a tool for predicting wildfire spread in peatlands, allow faster-than-real-time simulations, inform peatland management and thus can contribute to the mitigation of carbon emissions and haze-related adversities resulting from wildfires.

References

Alexander ME (1985) Estimating the length-to-breadth ratio of elliptical forest fire patterns. In '8th Conference on Fire and Forest Meteorology', Detroit, MI. pp. 287–304. (Society of American Foresters: Detroit, MI)

Alexandridis A, Vakalis D, Siettos CI, Bafas G V (2008) A cellular automata model for forest fire spread prediction: The case of the wildfire that swept through Spetses Island in 1990. *Applied Mathematics and Computation* **204**, 191–201. doi:10.1016/j.amc.2008.06.046

Alexandridis A, Russo L, Vakalis D, Bafas G V, Siettos CI (2011) Wildland fire spread modelling using cellular automata: Evolution in large-scale spatially heterogeneous environments under fire suppression tactics. *International Journal of Wildland Fire* **20**, 633–647. doi:10.1071/WF09119

Apers S, De Lannoy GJM, Baird AJ, Cobb AR, Dargie GC, del Aguila Pasquel J, Gruber A, Hastie A, Hidayat H, Hirano T, Hoyt AM, Jovani-Sancho AJ, Katimon A, Kurnain A, Koster RD, Lampela M, Mahanama SPP, Melling L, Page SE, Reichle RH, Taufik M, Vanderborght J, Bechtold M (2022) Tropical Peatland Hydrology Simulated With a Global Land Surface Model. *Journal Of Advances In Modeling Earth Systems* **14**, e2021MS002784. doi:10.1029/2021MS002784

Bechtold M, De Lannoy GJM, Koster RD, Reichle RH, Mahanama SP, Bleuten W, Bourgault MA, Brümmer C, Burdun I, Desai AR, Devito K, Grünwald T, Grygoruk M, Humphreys ER, Klatt J, Kurbatova J, Lohila A, Munir TM, Nilsson MB, Price JS, Röhl M, Schneider A, Tiemeyer B (2019) PEAT-CLSM: A Specific Treatment of Peatland Hydrology in the NASA Catchment Land Surface Model. *Journal of Advances in Modeling Earth Systems* **11**, 2130–2162. doi:10.1029/2018MS001574

Bechtold M, De Lannoy GJM, Reichle RH, Roose D, Balliston N, Burdun I, Devito K, Kurbatova J, Strack M, Zarov EA (2020) Improved groundwater table and L-band brightness temperature estimates for Northern Hemisphere peatlands using new model physics and SMOS observations in a global data assimilation framework. *Remote Sensing of Environment* **246**, 111805. doi:10.1016/j.rse.2020.111805

Belcher CM, Yearsley JM, Hadden RM, McElwain JC, Rein G (2010) Baseline intrinsic flammability of Earth's ecosystems estimated from paleoatmospheric oxygen over the past 350 million years. *Proceedings of the National Academy of Sciences* **107**, 22448–22453. doi:10.1073/pnas.1011974107

BMKG (2018) Data Online - Pusat Database. Available at https://dataonline.bmkg.go.id/data_iklim

Camps-Valls G, Campos-Taberner M, Moreno-Martínez Á, Walther S, Duveiller G, Cescatti A, Mahecha MD, Muñoz-Marí J, García-Haro FJ, Guanter L, Jung M, Gamon JA, Reichstein M, Running SW (2021) A unified vegetation index for quantifying the terrestrial biosphere. *Science Advances* **7**, eabc7447. doi:10.1126/sciadv.abc7447

Christensen EG, Fernandez-Anez N, Rein G (2020) Influence of soil conditions on the multidimensional spread of smouldering combustion in shallow layers. *Combustion and Flame* **214**, 361–370. doi:10.1016/j.combustflame.2019.11.001

Collin A, Bernardin D, Séro-Guillaume O (2011) A physical-based cellular automaton model for forest-fire propagation. *Combustion Science and Technology* **183**, 347–369. doi:10.1080/00102202.2010.508476

Copernicus (2022) Sentinel data, processed by the European Space Agency. Available at https://apps.sentinel-hub.com/eo-browser/?zoom=12&lat=-3.07853&lng=113.98528&themeId=DEFAULT-THEME&visualizationUrl=https%3A%2F%2Fservices.sentinel-hub.com%2Fogc%2Fwms%2Fbd86bcc0-f318-402b-a145-015f85b9427e&datasetId=S2L2A&fromTime=2018-09-28T00%3A00%3A00.000Z&toTime=2018-09-28T23%3A59%3A59.999Z&layerId=4-FALSE-COLOR-URBAN&demSource3D=%22MAPZEN%22

Dadap N (2020) Drainage Canals in Southeast Asian Peatland, Index Map. Stanford Digital Repository. Available at https://earthworks.stanford.edu/catalog/stanford-zy089tj2215

Favier C (2004) Percolation model of fire dynamic. *Physics Letters A* **330**, 396–401. doi:10.1016/j.physleta.2004.07.053

Fernandez-Anez N, Christensen K, Frette V, Rein G (2019) Simulation of fingering behavior in smoldering combustion using a cellular automaton. *Physical Review E* **99**, 023314. doi:10.1103/PhysRevE.99.023314

Ferraz A, Saatchi S, Xu L, Hagen S, Chave J, Yu Y, Meyer V, Garcia M, Silva C, Roswintiarti O, Samboko A, Sist P, Walker S, Pearson T, Wijaya A, Sullivan F, Rutishauser E, Hoekman D, Ganguly S (2019) 'Aboveground Biomass, Landcover, and Degradation, Kalimantan Forests, Indonesia, 2014.' (Oak Ridge National Laboratory Distributed Active Archive Center: Oak Ridge, TN, USA) 10.3334/ORNLDAAC/1645

Finney MA (1998) FARSITE: Fire Area Simulator – Model Development and Evaluation. (USDA Forest Service: MT)

Frandsen WH (1997) Ignition probability of organic soils. *Canadian Journal of Forest Research* **27**, 1471–1477. doi:10.1139/x97-106

Goldstein JE, Graham L, Ansori S, Vetrita Y, Thomas A, Applegate G, Vayda AP, Saharjo BH, Cochrane MA (2020) Beyond slash-and-burn: The roles of human activities, altered hydrology and fuels in peat fires in Central Kalimantan, Indonesia. *Singapore Journal of Tropical Geography* **41**, 190–208. doi:10.1111/sjtg.12319

Hu Y, Fernandez-Anez N, Smith TEL, Rein G (2018) Review of emissions from smouldering peat fires and their contribution to regional haze episodes. *International Journal of Wildland Fire* **27**, 293–312. doi:10.1071/WF17084

Huang X, Rein G (2015) Computational study of critical moisture and depth of burn in peat fires. *International Journal of Wildland Fire* **24**, 798–808. doi:10.1071/WF14178

Huang X, Rein G (2017) Downward spread of smouldering peat fire: The role of moisture, density and oxygen supply. *International Journal of Wildland Fire* **26**, 907–918. doi:10.1071/WF16198

Huang X, Restuccia F, Gramola M, Rein G (2016) Experimental study of the formation and collapse of an overhang in the lateral spread of smouldering peat fires. *Combustion and Flame* **168**, 393–402. doi:10.1016/j.combustflame.2016.01.017

Huijnen V, Wooster MJ, Kaiser JW, Gaveau DLA, Flemming J, Parrington M, Inness A, Murdiyarso D, Main B, Van Weele M (2016) Fire carbon emissions over maritime southeast Asia in 2015 largest since 1997. *Scientific Reports* **6**, 26886. doi:10.1038/srep26886

Islami N, Irianti M, Azhar, Nor M, Fakhrudin (2018) Geophysical survey for groundwater potential investigation in peat land area, Riau, Indonesia. *IOP Conference Series: Earth and Environmental Science* **144**, 012001. doi:10.1088/1755-1315/144/1/012001

Karafyllidis I, Thanailakis A (1997) A model for predicting forest fire spreading using cellular automata. *Ecological Modelling* **99**, 87–97. doi:10.1016/S0304-3800(96)01942-4

Khayal MSH, Khan A, Bashir S, Khan FH, Aslam S (2011) Modified new algorithm for seed filling. *Journal of Theoretical and Applied Information Technology* **26**, 28–32.

Lautenberger C (2013) Wildland fire modeling with an Eulerian level set method and automated calibration. *Fire Safety Journal* **62**, 289–298. doi:10.1016/j.firesaf.2013.08.014

Lin S, Sun P, Huang X (2019) Can peat soil support a flaming wildfire? *International Journal of Wildland Fire* **28**, 601–613. doi:10.1071/WF19018

Lin S, Liu Y, Huang X (2021) How to build a firebreak to stop smouldering peat fire: Insights from a laboratory-scale study. *International Journal of Wildland Fire* **30**, 454–461. doi:10.1071/WF20155

Null J (2021) 'El Niño and La Niña Years and Intensities.' (Golden Gate Weather Service)

Page SE, Siegert F, Rieley JO, Boehm HD V, Jaya A, Limin S (2002) The amount of carbon released from peat and forest fires in Indonesia during 1997. *Nature* **420**, 61–65. doi:10.1038/nature01131

Prat-Guitart N, Rein G, Hadden RM, Belcher CM, Yearsley JM (2016) Propagation probability and spread rates of self-sustained smouldering fires under controlled moisture content and bulk density conditions. *International Journal of Wildland Fire* **25**, 456–465. doi:10.1071/WF15103

Prat-Guitart N, Belcher CM, Thompson DK, Burns P, Yearsley JM (2017) Fine-scale distribution of moisture in the surface of a degraded blanket bog and its effects on the potential spread of smouldering fire. *Ecohydrology* **10**, e1898. doi:10.1002/eco.1898

Purnomo DMJ (2022) Cellular Automata Simulations of Field-Scale Flaming and Smouldering Wildfires in Peatlands. PhD thesis, Imperial College London, United Kingdom.

Purnomo DMJ, Bonner M, Moafi S, Rein G (2021) Using cellular automata to simulate field-scale flaming and smouldering wildfires in tropical peatlands. *Proceedings of the Combustion Institute* **38**, 5119–5127. doi:10.1016/j.proci.2020.08.052

Rein G (2013) Smouldering Fires and Natural Fuels. In 'Fire Phenomena and the Earth System'. (Ed. CM Belcher) pp. 15–33. (Wiley and Sons) doi:10.1002/9781118529539.ch2

Rein G, Huang X (2021) Smouldering wildfires in peatlands, forests and the arctic: Challenges and perspectives. *Current Opinion in Environmental Science & Health* **24**, 100296. doi:10.1016/j.coesh.2021.100296

Rezanezhad F, Price JS, Quinton WL, Lennartz B, Milojevic T, Van Cappellen P (2016) Structure of peat soils and implications for water storage, flow and solute transport: A review update for geochemists. *Chemical Geology* **429**, 75–84. doi:10.1016/j.chemgeo.2016.03.010

Ritzema H, Limin S, Kusin K, Jauhiainen J, Wösten H (2014) Canal blocking strategies for hydrological restoration of degraded tropical peatlands in Central Kalimantan, Indonesia. *Catena* **114**, 11–20. doi:10.1016/j.catena.2013.10.009

Rothermel RC (1972) A mathematical model for predicting fire spread in wildland fuels. USDA Forest Service, Intermountain Forest and Range Experiment Station, Research Paper INT-RP-115. (Ogden, UT) Available at https://www.fs.usda.gov/treesearch/pubs/32533

Scholten RC, Jandt R, Miller EA, Rogers BM, Veraverbeke S (2021) Overwintering fires in boreal forests. *Nature* **593**, 399–404. doi:10.1038/s41586-021-03437-y

Sofan P, Bruce D, Jones E, Khomarudin MR, Roswintiarti O (2020) Applying the tropical peatland combustion algorithm to Landsat-8 Operational Land Imager (OLI) and Sentinel-2 Multi Spectral Instrument (MSI) imagery. *Remote Sensing* **12**, 3958. doi:10.3390/rs12233958

Stavrakoudis D, Katagis T, Minakou C, Gitas IZ (2020) Automated Burned Scar Mapping Using Sentinel-2 Imagery. *Journal of Geographic Information System* **12**, 221–240. doi:10.4236/jgis.2020.123014

Sun L, Xu C, He Y, Zhao Y, Xu Y, Rui X, Xu H (2021) Adaptive forest fire spread simulation algorithm based on cellular automata. *Forests* **12**, 1431. doi:10.3390/f12111431

Turetsky MR, Benscoter B, Page S, Rein G, Van Der Werf GR, Watts A (2015) Global vulnerability of peatlands to fire and carbon loss. *Nature Geoscience* **8**, 11–14. doi:10.1038/ngeo2325

von Neumann J (1967) In 'Theory of Self-Reproducing Automata'. (Ed. AW Burks) (University of Illinois Press: Urbana) doi:10.2307/2005041

Waddington JM, Morris PJ, Kettridge N, Granath G, Thompson DK, Moore PA (2015) Hydrological feedbacks in northern peatlands. *Ecohydrology* **8**, 113–127. doi:10.1002/eco.1493

Widyastuti K, Imron MA, Pradopo ST, Suryatmojo H, Sopha BM, Spessa A, Berger U (2021) PeatFire: an agent-based model to simulate fire ignition and spreading in a tropical peatland ecosystem. *International Journal of Wildland Fire* **30**, 71–89. doi:10.1071/WF19213

Wolfram S (1984) Cellular automata as models of complexity. *Nature* **311**, 419–424. doi:10.1038/311419a0

Yuan H, Restuccia F, Rein G (2021) Spontaneous ignition of soils: A multi-step reaction scheme to simulate self-heating ignition of smouldering peat fires. *International Journal of Wildland Fire* **30**, 440–453. doi:10.1071/WF19128

Data availability. The data that support this study are available on request.

Conflicts of interests. The authors declare no conflicts of interest.

Declaration of funding. This research was sponsored by European Research Council (ERC) Consolidator Grant HAZE (682587), Indonesian Endowment Fund for Education (LPDP), and by the Research Foundation Flanders (FWO, G095720N). Computer resources and services used for PEATCLSM simulations were provided by the High Performance Computing system of the Vlaams Supercomputer Center funded by FWO and the Flemish Government.

Author affiliations
[A]Department of Mechanical Engineering, Leverhulme Centre for Wildfires, Environment and Society, Imperial College London, London, SW7 2AZ, UK.
[B]Department of Earth and Environmental Sciences, KU Leuven, Heverlee, Belgium.
[C]Research Center for Remote Sensing, National Research and Innovation Agency of Indonesia (BRIN), Jakarta, Indonesia.

Appendix

Ellipse parameters

The formulation of the ellipse perimeter used in the model to estimate the effect of wind on flames (Eqn 3) is shown below:

$$a = \left(\frac{r_H + 1}{2r_L r_H}\right);\ b = \left(\frac{r_H + 1}{2r_H}\right);\ c = \left(b - \frac{1}{r_H}\right) \tag{A1}$$

$$r_L = 0.936e^{0.2566U} + 0.461e^{-0.1548U} - 0.397 \tag{A2}$$

$$r_H = \frac{r_L + (r_L{}^2 - 1)^{0.5}}{r_L - (r_L{}^2 - 1)^{0.5}} \tag{A3}$$

where r_L is length to breadth ratio, r_H is head to back ratio, and U is wind speed.

Recursive burning rule of flaming wildfires

The cells with *FV* states transition to become either *EP* or *SP* after several time steps. If the transition happens after too few time steps, the spread of the flaming wildfire is not sustained, whereas if the transition happens after too many time steps, the flaming wildfires are sustained for too long, which violates the observed phenomena. We found that by using a probability of *FV* cells changing their state between $5P_f$ and $25P_f$, flaming wildfires were sustained but not for too long. The long-sustained flaming wildfires are indicated by a wide flaming vegetation front. We determined that this width is less than 10 cells. This value was selected based on the width that facilitated a continuous flaming vegetation layer. With less than 10 cells flaming vegetation width, the perimeter of the flaming vegetation is disconnected at several locations, which correspond to the unburned vegetation. Therefore, once the width of flaming vegetation layer exceeds 10 cells, the flaming wildfire can be considered as being sustained for too long. Between $5P_f$ and $25P_f$, the value of φ to maintain the accuracy of the model against Rothermel model calculations does not significantly change. Therefore, we selected the middle value, in which the *FV* cells transition to either *EP* or *SP* at the subsequent time step with a probability of $15P_f$. However, this value changes to become $15P_f\exp(0.2\sigma)$ when there is rain, where σ is precipitation, as adapted from Alexandridis *et al.* (2011).

Table A1. Values of input parameters used to calculate flaming spread rate of three surface vegetation classes present in the landscape under study.

Input parameters	Dry shrub	Wet shrub	Trees
Particle surface area to volume ratio (1/m)	4921	4921	4921
Oven-dry fuel loading (kg/m^2)	0.45	0.45	0.89
Fuel depth (m)	0.61	0.61	0.71
Fuel MC	0.2	0.23	0.2
Oven-dry particle density (kg/m^3)	512	512	512
Particle total mineral content	0.0555	0.0555	0.0555
Particle low heat content (kJ/kg)	18 608	18 608	18 608
MC of extinction	0.3	0.3	0.3
Particle effective mineral content	0.01	0.01	0.01

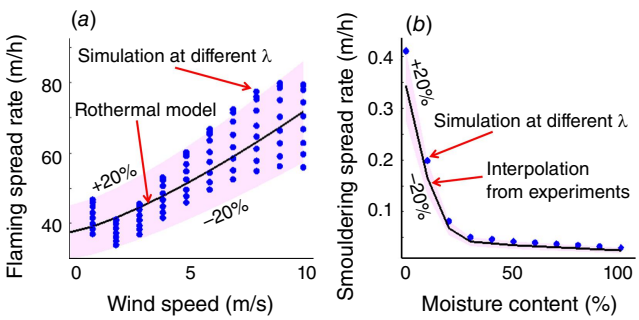

Fig. A1. (*a*) Comparison of flaming spread rate with different wind speed between the Rothermel model and the KAPAS II simulations at different spatiotemporal resolutions (λ). (*b*) Comparison of smouldering spread rate with different moisture content between the experiments of Huang *et al.* (2016), Prat-Guitart *et al.* (2016) and the KAPAS II simulations at different spatiotemporal resolution (λ).

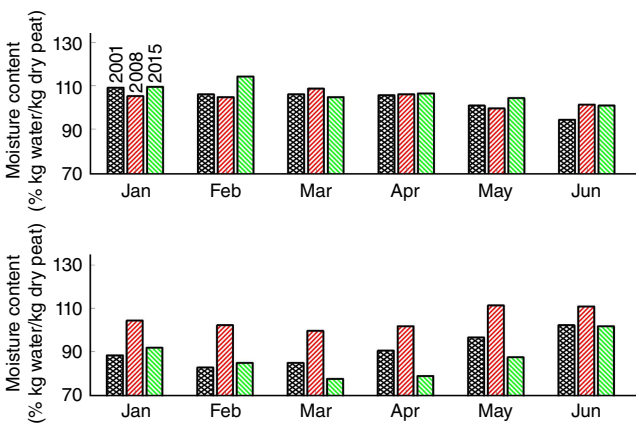

Fig. A2. Examples of the gravimetric MC of peat in Borneo in different years, as simulated with the model proposed by Apers *et al.* (2022). Each bar represents the average peat MC in 1 month. The El Niño event that occurred in the year 2015 is clearly reflected in the low MC values identified during the dry season, as shown with green bars.